

OPTICAL–INFRARED PROPERTIES OF FAINT 1.3 MM SOURCES DETECTED WITH ALMA

BUNYO HATSUKADE^{1*}, KOUJI OHTA², KIYOTO YABE^{1,3}, AKIFUMI SEKO², RYU MAKIYA⁴, AND MASAYUKI AKIYAMA⁵,¹National Astronomical Observatory of Japan, 2-21-1 Osawa, Mitaka, Tokyo 181-8588, Japan²Department of Astronomy, Kyoto University, Kyoto 606-8502, Japan³Kavli Institute for the Physics and Mathematics of the Universe (WPI), The University of Tokyo, 5-1-5 Kashiwanoha, Kashiwa, Chiba 277-8583, Japan⁴Institute of Astronomy, University of Tokyo, 2-21-1 Osawa, Mitaka, Tokyo 181-0015, Japan⁵Astronomical Institute, Tohoku University, Aramaki, Aoba-ku, Sendai, Miyagi 980-8578, Japan

Received 2015 February 12; accepted 2015 July 31

ABSTRACT

We report optical-infrared (IR) properties of faint 1.3 mm sources ($S_{1.3\text{mm}} = 0.2\text{--}1.0$ mJy) detected with the Atacama Large Millimeter/submillimeter Array (ALMA) in the Subaru/XMM-Newton Deep Survey (SXDS) field. We searched for optical/IR counterparts of 8 ALMA-detected sources ($\geq 4.0\sigma$, the sum of the probability of spurious source contamination is ~ 1) in a K -band source catalog. Four ALMA sources have K -band counterpart candidates within a $0''.4$ radius. Comparison between ALMA-detected and undetected K -band sources in the same observing fields shows that ALMA-detected sources tend to be brighter, more massive, and more actively forming stars. While many of the ALMA-identified submillimeter-bright galaxies (SMGs) in previous studies lie above the sequence of star-forming galaxies in stellar mass–star-formation rate plane, our ALMA sources are located in the sequence, suggesting that the ALMA-detected faint sources are more like ‘normal’ star-forming galaxies rather than ‘classical’ SMGs. We found a region where multiple ALMA sources and K -band sources reside in a narrow photometric redshift range ($z \sim 1.3\text{--}1.6$) within a radius of $5''$ (42 kpc if we assume $z = 1.45$). This is possibly a pre-merging system and we may be witnessing the early phase of formation of a massive elliptical galaxy.

Subject headings: galaxies: evolution — galaxies: formation — galaxies: high-redshift — galaxies: ISM — cosmology: observations — submillimeter: galaxies

1. INTRODUCTION

Since the fraction of dust-obscured star formation to the total star formation increases with redshift (e.g., Takeuchi et al. 2005; Le Floch et al. 2005), observations at infrared (IR) to millimeter/submillimeter (mm/submm) wavelengths are essential to understand the cosmic star formation history and the galaxy evolution. Deep and wide-field surveys uncovered a new population of mm/submm-bright galaxies at high redshifts (SMGs) (see Blain et al. 2002, for a review). SMGs are highly obscured by dust, and the resulting thermal dust emission dominates the bolometric luminosity. The energy source of mm/submm emission is primarily from intense star formation activity, with star-formation rates (SFRs) of $10^2\text{--}10^3 M_\odot \text{yr}^{-1}$. The heavy dust obscuration in SMGs makes it difficult to understand their optical/near-infrared (NIR) properties. In addition, the coarse angular resolution of single dish telescopes ($\gtrsim 15''$) prevents from identifying optical/NIR counterparts. One of the most successful ways to identify counterparts is to obtain high resolution, deep radio imaging (e.g., Ivison et al. 1998, 2002). Deep radio observations with interferometers reveal robust radio counterparts of $\sim 50\%\text{--}80\%$ of SMGs (e.g., Ivison et al. 2005, 2007). A problem in radio identification is the rapid dimming of radio flux of galaxies with increasing redshift. The most accurate means of achieving high precision astrometry of SMGs is to use interferometers at mm/submm (e.g., Iono et al. 2006; Wang et al.

2007; Younger et al. 2007, 2008, 2009; Hatsukade et al. 2010), although this approach needs much time to detect an object compared to the radio imaging. The advent of the Atacama Large Millimeter/submillimeter Array (ALMA) has changed this situation thanks to its high sensitivity and high angular resolution.

Optical/NIR follow-up observations and spectral energy distribution (SED) model fits have shown that SMGs have substantial stellar masses of $\sim 10^{11}\text{--}10^{12} M_\odot$ (e.g., Smail et al. 2004; Borys et al. 2005; Dye et al. 2008; Michałowski et al. 2010; Hainline et al. 2011). It is thought that SMGs are progenitors of massive elliptical galaxies in the present-day universe observed during their formation phase (e.g., Lilly et al. 1999; Smail et al. 2004; Simpson et al. 2014). It is known that star-forming galaxies follow a tight correlation between stellar mass and SFR (star-forming main sequence; e.g., Noeske et al. 2007), and SMGs are found to be located above the main sequence or at the massive end of the main sequence (e.g., Daddi et al. 2007; da Cunha et al. 2015). These suggest that previous mm/submm surveys trace only a small fraction of star-forming galaxies. This is inferable by the fact that SMGs detected in previous blank-field surveys contribute the extragalactic background light, which is the integral of unresolved emission from extragalactic sources, by only $\sim 20\%\text{--}40\%$ at $850 \mu\text{m}$ (e.g., Barger et al. 1999; Borys et al. 2003; Coppin et al. 2006) and $\sim 10\%\text{--}20\%$ at 1 mm (e.g., Greve et al. 2004; Scott et al. 2008, 2010; Hatsukade et al. 2011). In order to understand the cosmic star-formation history and galaxy evolution, it is necessary to study fainter mm/submm sources ($S_{1\text{mm}} \lesssim 1$ mJy), which con-

bunyo.hatsukade@nao.ac.jp

* NAOJ Fellow

nect ‘classical’ SMGs and ‘normal’ star-forming galaxies. However, since the previous surveys of SMGs were conducted with single-dish telescopes, it has been very hard to detect fainter sources because of the limited sensitivity and the source confusion except for rare samples around gravitational lensing clusters (e.g., Chen et al. 2014), and it is still unclear the optical/NIR properties of fainter mm/submm sources. ALMA enables us to detect fainter sources with the flux densities about an order of magnitude fainter than those detected in previous single-dish surveys, allowing us to study the properties of faint mm/submm sources (e.g., Hatsukade et al. 2013; Ono et al. 2014; Fujimoto et al. 2015). In this paper, we present the optical–IR properties of ALMA-detected faint sources ($S_{1.3\text{mm}} = 0.2\text{--}1.0$ mJy). The arrangement of this paper is as follows. Section 2 outlines the data we used. Section 3 describes the method of counterpart identification. In Section 4, we discuss the optical–IR properties of the ALMA-detected sources. A summary is presented in Section 5. Throughout the paper, we adopt a cosmology with $H_0 = 70$ km s $^{-1}$ Mpc $^{-1}$, $\Omega_M = 0.3$, and $\Omega_\Lambda = 0.7$. All magnitudes are in the AB system (Oke & Gunn 1983).

2. DATA

We conducted ALMA band 6 observations toward 20 star-forming galaxies at $z \sim 1.4$ in the Subaru/XMM-Newton Deep Survey (SXDS) field (Furusawa et al. 2008). The targets were extracted from a stellar mass limit ($>10^{9.5} M_\odot$) sample whose redshifts and H α SFR were obtained by near-infrared (NIR) spectroscopy with the Fibre Multi-Object Spectro-graph (FMOS; Kimura et al. 2010) on the Subaru telescope (Yabe et al. 2012, 2014). The ALMA observations were carried out in August 2012 with 23–25 antennas during the cycle 0 session. The correlator was used in the frequency domain mode with a bandwidth of 1875 MHz (488.28 kHz \times 3840 channels). We obtained 20 pointings centered on the 20 targets, each with on-source observing time of 8–15 minutes. The full width at half maximum (FWHM) of the primary beam is $\sim 26''$.

The data were reduced with the Common Astronomy Software Applications (CASA; McMullin et al. 2007) package in a standard manner. We found that the coordinates of a phase calibrator were wrong (by $\sim 0.3''$) in the originally delivered data, which causes positional offsets of sources detected in science maps. We re-calibrated the data by modifying the phase center of the visibilities of the phase calibrator manually to obtain the correct coordinates in the final science maps. We used the 2012 models of Solar System Object for flux calibrations instead of the 2010 models used in Hatsukade et al. (2013), which makes the flux density of the maps at most 15% smaller. The maps were processed with the CLEAN algorithm with the natural weighting, which gives the final synthesized beamsizes of $\sim 0''.6\text{--}1''.3$. The continuum images of the 20 fields are created with the rms noise level of 0.04–0.10 mJy beam $^{-1}$.

We used the area within the primary beam of the images for source detection. Source extraction was conducted on the 20 continuum images (before primary beam correction) where all the sources with a peak signal-to-noise ratio (SN) above 3.5 were CLEANed. The probability of contamination by spurious sources

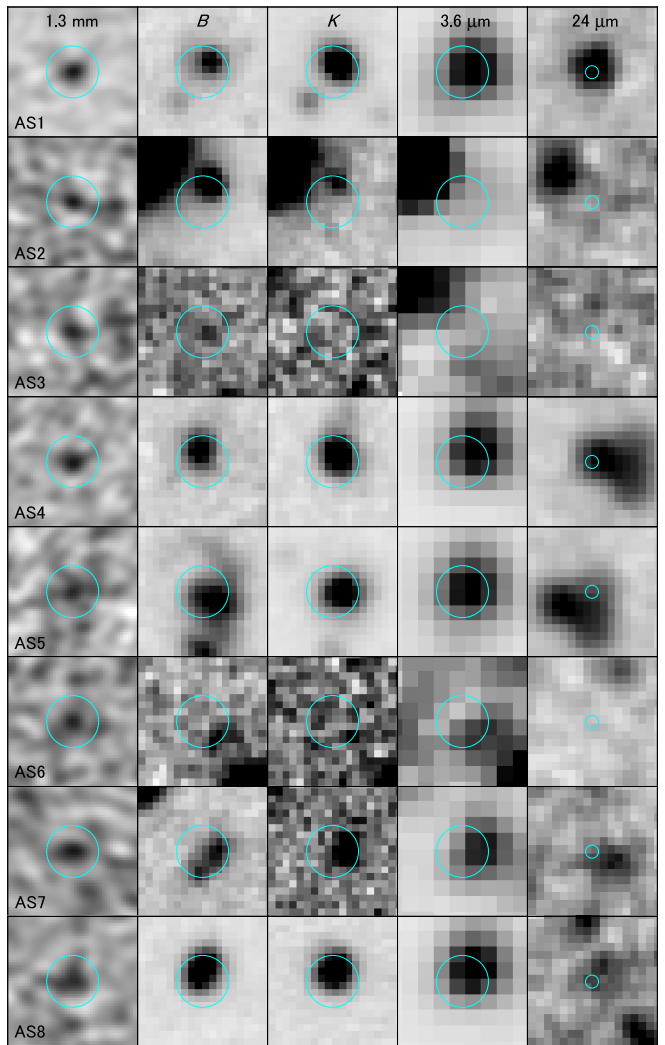


FIG. 1.— Multi-wavelength images of the ALMA sources. Panels from left to right are ALMA 1.3 mm, Subaru/Suprime-Cam B , UKIRT/WFCAM K_s , *Spitzer*/IRAC 3.6 μm , and MIPS 24 μm . The size of each panel is $5'' \times 5''$ for the first four panels, and $20'' \times 20''$ for the last panel. Circles with $1''$ radius centered on the ALMA sources are presented in each panel.

(C_{spurious}) is estimated by counting the negative peaks in each map as a function of SN and averaged over the 20 images (Hatsukade et al. 2013). In this paper, we adopt the detection threshold of $\text{SN} \geq 4.0$, where C_{spurious} is less than 0.5. We detected 8 sources at $\text{SN} \geq 4.0$, of which three sources are the original targets of ALMA observations and five sources are serendipitously-detected sources. The source list is presented in Table 1¹. The peak flux density of the continuum sources corrected for the primary beam attenuation is $S_{1.3\text{mm}} = 0.17\text{--}1.0$ mJy ($4.0\text{--}13\sigma$). Note that the source sizes in the images (without deconvolution) are not significantly smaller than the synthesized beamsizes. In this study, we adopt the continuum flux density measured without excluding channels where CO emission lines present to be fairly compared with past and future studies in the continuum where the contamination is unknown.

¹ Two sources (AS2 and AS4) are also detected by Fujimoto et al. (2015).

TABLE 1
ALMA-DETECTED SOURCES

Name	ID	R.A. (J2000)	Decl. (J2000)	$S_{1.3\text{mm}}^a$ (mJy)	SN	C_{spurious}^b	Note
ALMA_SXDS1_13015_1	AS1	02 17 13.63	-05 09 40.0	1.00 ± 0.08	13	0.0	original target
ALMA_SXDS1_31189_1	AS2	02 17 13.33	-05 04 02.3	0.30 ± 0.06	4.8	0.0	serendipitous
ALMA_SXDS1_31189_2	AS3	02 17 13.82	-05 04 18.7	0.35 ± 0.08	4.3	0.1	serendipitous
ALMA_SXDS1_59863_1	AS4	02 17 46.27	-04 54 39.8	0.53 ± 0.09	6.0	0.0	serendipitous
ALMA_SXDS1_59863_2	AS5	02 17 45.89	-04 54 37.4	0.30 ± 0.07	4.0	0.4	original target
ALMA_SXDS1_79307_1	AS6	02 17 06.02	-04 51 37.5	0.36 ± 0.09	4.1	0.3	serendipitous
ALMA_SXDS3_110465_1	AS7	02 18 21.27	-05 19 06.9	0.39 ± 0.08	4.8	0.0	serendipitous
ALMA_SXDS5_28019_1	AS8	02 16 08.53	-05 06 15.8	0.17 ± 0.04	4.4	0.1	original target

NOTE. — ^a 1.3 mm flux density corrected for primary beam attenuation. ^b Probability of contamination by spurious sources.

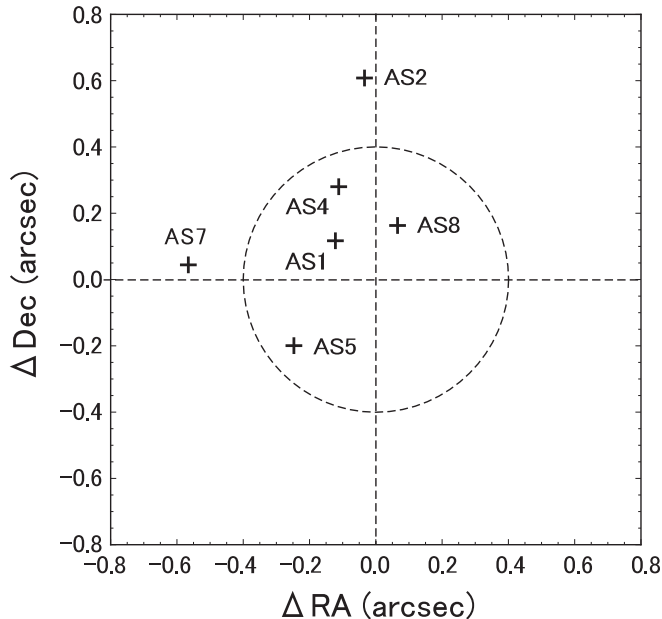


FIG. 2.— Positional offsets of the K -band counterpart candidates from the ALMA sources. The dashed circle represents the offset of $0''.4$, which is the maximum expected positional offset between the ALMA sources and K -band counterparts.

3. COUNTERPART IDENTIFICATION

Optical/IR counterparts for the ALMA sources are searched in the K -band-selected source catalog of Yabe et al. (2012, 2014). The limiting magnitude of the catalog is $K_s = 24.6$ mag ($2''.0$ aperture, 5σ), and the WCS accuracy of the source coordinates is $\sim 0''.2$ – $0''.3$ (rms). The synthesized beam size of the ALMA observations is $\sim 0''.6$ – $1''.3$ (major axis FWHM), and the expected astrometric accuracy of the ALMA sources is $\sim 0''.06$ – $0''.3$ (\sim FWHM/SN). Therefore, the expected positional accuracy between K -band and ALMA coordinates is $\sim 0''.3$ – $0''.4$ as the square-root of sum of squares of both accuracies. Hodge et al. (2013) compared ALMA-detected SMGs with VLA 1.4 GHz counterparts and found that the positions are accurate to within $0''.2$ – $0''.3$. The average positional offsets between ALMA-detected SMGs and HST counterparts are found to be $0''.3$ – $0''.4$ (Wiklind et al. 2014; Chen et al. 2015). The positions of mm/submm emission and K -band emission, which typically trace dust-obscured and unobscured part, respectively, are not necessarily coincide in a galaxy (e.g., Iono et al. 2006; Chen et al. 2015; Hodge et al. 2015; Hatsukade et al. 2015). Figure 1

shows the 1.3 mm image for the 8 ALMA sources together with multi-wavelength images of Subaru/Suprime-Cam B (Furusawa et al. 2008), UKIRT/Wide Field Camera (WFCAM) K_s (Lawrence et al. 2007), *Spitzer*/Infrared Array Camera (IRAC) $3.6 \mu\text{m}$, and MIPS $24 \mu\text{m}$ (Dunlop et al. in preparation). We found K -band counterpart candidates for 6 out of the 8 ALMA sources within a radius of $1''$. AS3 and AS6 have faint emission in the B -band image, but they are not detected in K -band. The positional offset between the ALMA sources and their K -band counterpart candidates is shown in Figure 2. AS2 and AS7 have a larger offset ($0''.5$ – $0''.6$) than the expected positional accuracy of $\sim 0''.3$ – $0''.4$, and we regard them as unidentified. The average offset for the remaining four ALMA sources is $(\Delta RA, \Delta Dec) = (-0''.10 \pm 0''.13, +0''.09 \pm 0''.20)$, which is within the expected positional accuracy between K -band and ALMA coordinates.

We identified K -band counterparts for four out of the 8 ALMA sources. If we focus on the serendipitous sources, counterparts are found for 1 out of 5 sources. One possibility for not having K -band counterparts is that the ALMA sources are spurious. The sum of C_{spurious} of the 8 ALMA sources is ~ 1 (Table 1), suggesting that at least one source is spurious. Another possibility is that they are obscured by dust or at higher redshift, which could make the optical/NIR emission fainter than the limiting magnitude of our K -band source catalog (Chen et al. 2014). The faint B -band emission in AS3 and AS6 may be from less obscured regions within the sources. While we expect emission at mid-IR if they have dust-obscured star-forming regions, they are not detected with *Spitzer*, suggesting that they may be at higher redshift if not spurious.

4. DISCUSSION

4.1. Optical–IR Properties

For the ALMA sources with K -band counterparts, we investigate the optical–IR properties. Fig. 3 shows a K -band and IRAC color-magnitude diagram (K_s versus $K_s - 3.6 \mu\text{m}$) (left) and a IRAC color-color diagram ($m_{3.6\mu\text{m}} - m_{4.5\mu\text{m}}$ versus $m_{5.8\mu\text{m}} - m_{8.0\mu\text{m}}$) (right) for the ALMA sources. For comparison, K -band sources at $1.0 < z < 2.0$ in the catalog of Yabe et al. (2014) are plotted. We also show SMGs identified in the ALMA follow-up observations of the LABOCA Extended Chandra Deep Field South surveys (ALESS). The ALESS SMGs in the same redshift range ($1.0 < z < 2.0$) are taken from Simpson et al. (2014). The plots show that our ALMA sources are bluer in $K_s - m_{3.6\mu\text{m}}$ and

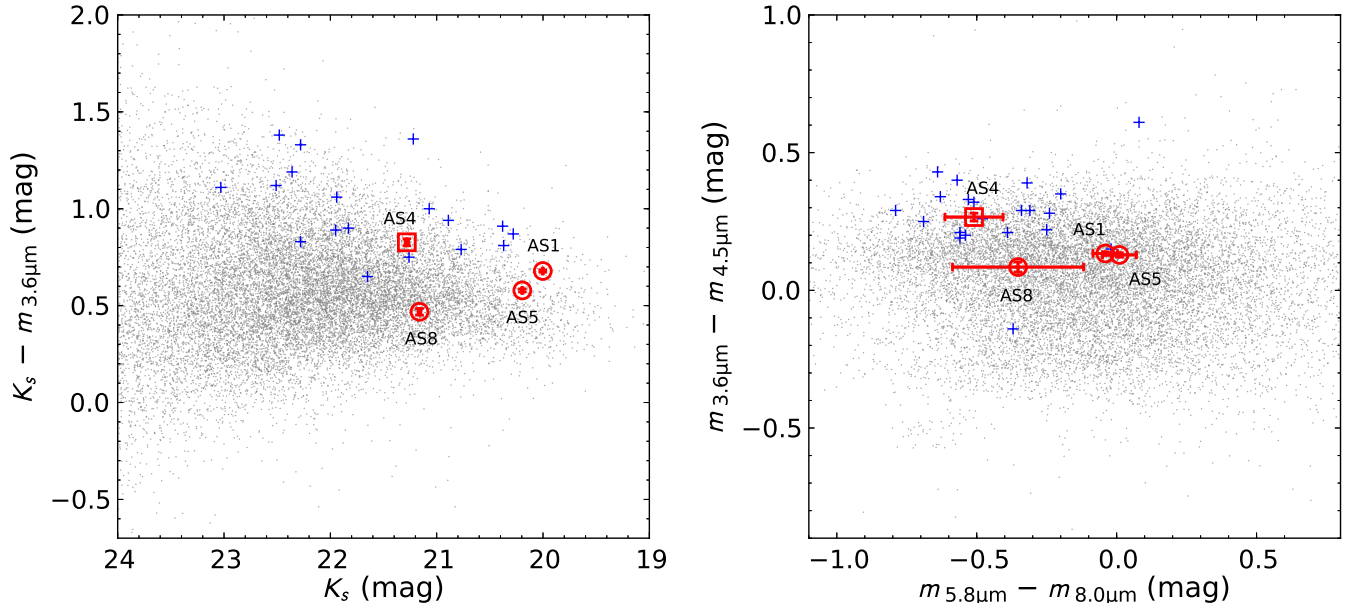


FIG. 3.— K -band and IRAC color-magnitude diagram (K_s versus $K_s - 3.6 \mu\text{m}$) (left) and IRAC color-color diagram ($m_{3.6\mu\text{m}} - m_{4.5\mu\text{m}}$ versus $m_{5.8\mu\text{m}} - m_{8.0\mu\text{m}}$) (right). The ALMA sources identified with the original FMOS targets and the ALMA serendipitous source are presented as circles and squares, respectively. For comparison, we plot ALMA-identified SMGs of Simpson et al. (2014) (crosses) and K -band sources in the catalog of Yabe et al. (2014) (dots) at a spectroscopic (if available) or photometric redshift range of $1.0 < z < 2.0$.

$m_{3.6\mu\text{m}} - m_{4.5\mu\text{m}}$ compared to the ALESS SMGs.

We estimated physical quantities for our ALMA sources. The photometric redshift and the stellar mass are derived from SED fits to far-UV–mid-IR data of Galaxy Evolution Explorer (GALEX) far- and near-UV, CFHT/MegaCam u , Subaru/Suprime-Cam B , V , R_C , i' , and z , UKIRT/WFCAM J , H and K_s , *Spitzer*/IRAC $3.6 \mu\text{m}$, $4.5 \mu\text{m}$, $5.8 \mu\text{m}$, and $8.0 \mu\text{m}$. The Salpeter IMF (Salpeter 1955) with a mass range of 0.1 – $100 M_\odot$ was assumed. The color excess was derived from the rest-frame UV color, and the SFR was derived from the rest-frame UV luminosity density corrected for extinction by using the color excess (see Yabe et al. 2012, 2014, for details). The quantities are summarized in Table 2. The standard deviation of the difference between photometric and spectroscopic redshifts in the sample of Yabe et al. (2014) is $\sigma \sim 0.05$. We adopt $\Delta z = 0.05$ for the error of photometric redshifts. We note that the ALMA observing fields were centered on $z \sim 1.4$ star-forming galaxies, which could be biased regions. To eliminate such a bias completely, it is essential to observe ‘purely’ blank fields. In Figure 4, we compared the stellar mass and SFR of our ALMA sources and the ALESS SMGs at $1.0 < z < 2.0$. While more than half of the ALESS SMGs are above the main sequence (da Cunha et al. 2015), the ALMA serendipitous source is located in the main sequence. This suggests that ALMA-detected faint sources are likely to have properties similar to normal star-forming galaxies (Hatsukade et al. 2013; Ono et al. 2014; Fujimoto et al. 2015).

4.2. ALMA-detected and undetected sources

To see whether there is a common characteristic in sources that are detected with ALMA, we compared the properties of K -band sources detected and unde-

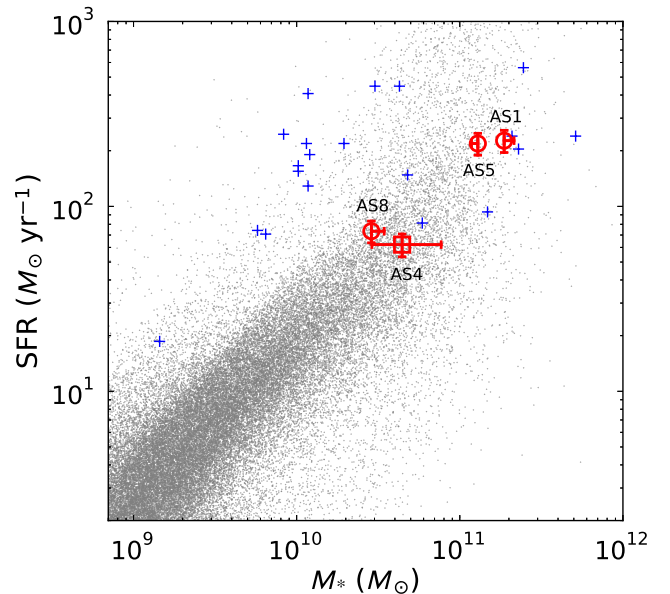


FIG. 4.— Comparison of stellar mass and SFR for the ALMA sources, ALMA-identified SMGs (da Cunha et al. 2015), and the K -band sources. Symbols are the same as in Fig. 3. The ALMA-identified SMGs and K -band sources are at a redshift range of $1.0 < z < 2.0$.

tected with ALMA within the field of views of ALMA observations. In Figure 5, we plot K -band magnitude, stellar mass, and SFR as a function of redshift. The plots show that the ALMA-detected sources tend to be brighter, more massive, and more actively star-forming galaxies among the K -band sources. We show the expected SFR for a source with $S_{1.3\text{mm}} = 0.2 \text{ mJy}$ (the faintest flux density of our ALMA sources) as a function of redshift in the right panel of Fig-

TABLE 2
PHYSICAL PROPERTIES OF ALMA-DETECTED SOURCES WITH K -BAND COUNTERPART CANDIDATES

ID	offset ^a (arcsec)	K_s (mag)	z_{spec}	z_{phot}	$E(B-V)$ (mag)	M_* (M_\odot)	SFR(UV SED) ($M_\odot \text{ yr}^{-1}$)
AS1	0.17	20.00 ± 0.00	1.451	1.42 ± 0.05	$0.50^{+0.00}_{-0.05}$	$1.87^{+0.28}_{-0.00} \times 10^{11}$	227 ± 31
AS4 ^b	0.30	21.28 ± 0.02	—	1.53 ± 0.05	$0.60^{+0.05}_{-0.10}$	$4.43^{+3.26}_{-1.54} \times 10^{10}$	62 ± 9
AS5	0.32	20.19 ± 0.01	1.448	1.43 ± 0.05	$0.45^{+0.05}_{-0.00}$	$1.29^{+0.00}_{-0.11} \times 10^{11}$	219 ± 30
AS8	0.18	21.16 ± 0.01	1.348	1.32 ± 0.05	$0.35^{+0.05}_{-0.00}$	$2.87^{+0.57}_{-0.00} \times 10^{10}$	73 ± 10

NOTE. — ^a Positional offset between ALMA source and K -band counterpart candidate. ^b Serendipitous source.

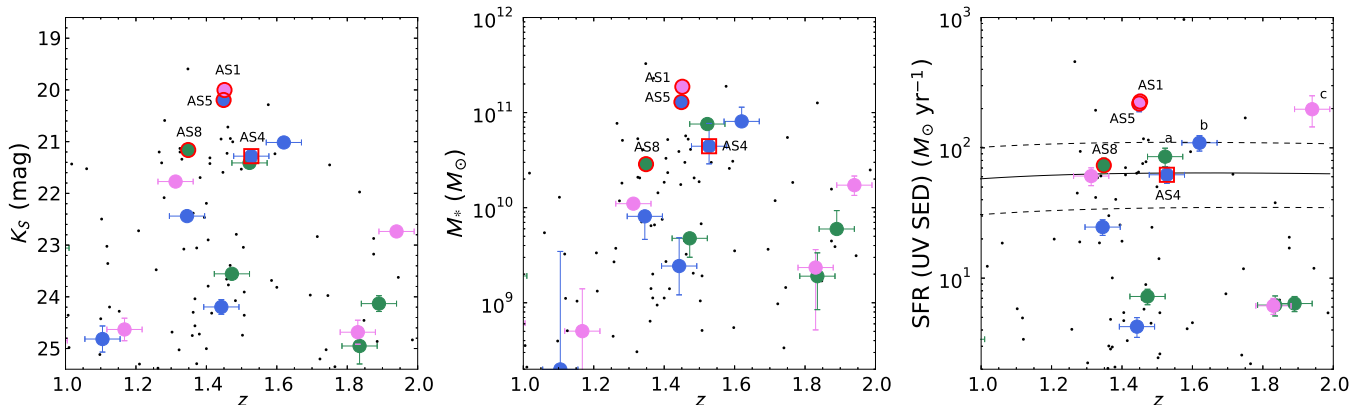


FIG. 5.— K_s magnitude, stellar mass, and SFR of K -band sources within the field of ALMA observations as a function of redshift. The ALMA sources identified with the original FMOS targets and the ALMA serendipitous source are presented as red circles and squares, respectively. K -band sources in the field of views where ALMA sources are detected are shown as large circles; different colors represent different fields. K -band sources in the field of views where no ALMA sources are detected are shown as dots. The redshifts are spectroscopic (if available) or photometric. The errors on photometric redshifts ($\Delta z = 0.05$) are presented in the horizontal axis. In the right panel, we present SFR as a function of redshift expected for a source with $S_{1.3\text{mm}} = 0.2$ mJy, $T_{\text{dust}} = 35 (\pm 5)$ K, and $\beta = 1.5$ as a solid (dashed) line.

ure 5. We estimate the SFR by using the SFR–far-IR (FIR) luminosity (L_{FIR}) relation of Kennicutt (1998). We derived FIR luminosity from $L_{\text{FIR}} = 4\pi M_{\text{dust}} \int_0^\infty \kappa_d(\nu_{\text{rest}}) B(\nu_{\text{rest}}, T_{\text{dust}}) d\nu$ and dust mass from $M_{\text{dust}} = S_{\text{obs}} D_L^2 / [(1+z)\kappa_d(\nu_{\text{rest}}) B(\nu_{\text{rest}}, T_{\text{dust}})]$ (De Breuck et al. 2003), where $\kappa_d(\nu_{\text{rest}})$ is the dust mass absorption coefficient, ν_{rest} is the rest-frame frequency, T_{dust} is the dust temperature, $B(\nu_{\text{rest}}, T_{\text{dust}})$ is the Planck function, S_{obs} is the observed flux density, and D_L is the luminosity distance. We assume that the absorption coefficient varies as $\kappa_d \propto \nu^\beta$ and the emissivity index lies between 1 and 2 (e.g. Hildebrand 1983). We adopt $\kappa_d(125 \mu\text{m}) = 2.64 \pm 0.29 \text{ m}^2 \text{ kg}^{-1}$ (Dunne et al. 2003), $\beta = 1.5$, and $T_{\text{dust}} = 30\text{--}40$ K, typical value for $z \sim 0\text{--}2$ star-forming galaxies (e.g., Elbaz et al. 2011; Symeonidis et al. 2013). The solid and dashed lines indicate that sources with $S_{1.3\text{mm}} \geq 0.2$ mJy above the lines can be detected with the ALMA observations based on the assumption that the SFRs derived from UV continuum and dust emission are consistent. There are K -band sources within or above the lines which are not detected with ALMA (labeled as a, b, and c in Figure 5 (right)). Source a is located in the same field as AS8. While AS8 is located at the field center, source a is $\sim 10''$ away from the field center, where the sensitivity is $\sim 35\%$ lower than that at the field center, suggesting that the lower sensitivity missed source a. Source b is seen in the ALMA image, but the SN of 3.9 is lower than the threshold of 4.0 adopted in this study. Around this source, two

ALMA sources (AS4 and AS5) are detected within a narrow redshift range, suggesting that star-forming activity is enhanced by the interaction (see Section 4.3). Source c is located $\sim 3''$ away from the center of the same field as AS1, where the rms noise level ($0.08 \text{ mJy beam}^{-1}$) is higher among the ALMA observing fields. In spite of the higher SFR, source c was not detected with ALMA, suggesting the SFR has uncertainty. We also investigated the properties of K -band sources above the the expected SFR line in Fig. 5 in the field of views where no ALMA sources are detected, and found that the non-detection with ALMA can be explained by lower sensitivity, or lower SFRs than those of ALMA sources with the uncertainty of SFRs estimated both from UV continuum and dust emission.

4.3. Overdense around ALMA sources

We found a region where multiple ALMA sources and K -band sources reside in a small projected area (Figure 6, Table 3). Five K -band sources are located within a radius of $5''$ (42 kpc if we assume $z = 1.45$), of which two sources are the ALMA sources (AS4 and AS5). SXDS1_59617 is also presented in the ALMA 1.3 mm image with SN = 3.9. Although the probability of contamination by spurious sources for SXDS1_59617 is 0.9 due to the low SN, the detection in other bands (B or $Spitzer$) suggests that the source is real. AS5 is the original target for ALMA observations, whose spectroscopic redshift is $z_{\text{spec}} = 1.448$. The spectroscopic or photometric redshifts of four sources (AS4, AS5, SXDS1_59617

TABLE 3
PHYSICAL PROPERTIES OF K -BAND SOURCES IN THE OVERDENSE REGION

K -band ID	$S_{1.3\text{mm}}$ (mJy)	C_{spurious}	K_s (mag)	z_{phot}	$E(B-V)$ (mag)	M_* (M_{\odot})	SFR(UV SED) ($M_{\odot} \text{ yr}^{-1}$)
SXDS1_59617	0.33 ± 0.09	0.9	21.02 ± 0.02	1.62 ± 0.05	$0.35^{+0.00}_{-0.05}$	$8.08^{+3.32}_{-0.74} \times 10^{10}$	109 ± 15
SXDS1_60181	$<0.23^*$	—	22.44 ± 0.04	1.35 ± 0.05	$0.40^{+0.05}_{-0.00}$	$8.11^{+0.79}_{-3.47} \times 10^9$	25 ± 3
SXDS1_60394	$<0.23^*$	—	23.55 ± 0.09	2.37 ± 0.05	$0.55^{+0.05}_{-0.05}$	$7.05^{+6.85}_{-2.34} \times 10^9$	134 ± 30

NOTE. — * 3σ upper limit.

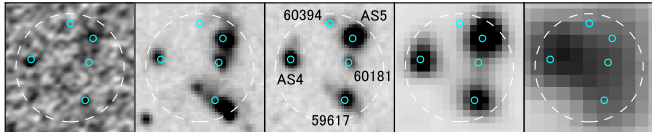


FIG. 6.— Multi-wavelength images around the multiple ALMA sources. From left to right: ALMA 1.3 mm, Subaru/Suprime-Cam B , UKIRT/WFCAM K_s , *Spitzer*/IRAC $3.6 \mu\text{m}$, and MIPS $24 \mu\text{m}$. The dashed circle shows a region within a radius of $5''$ (42 kpc at $z = 1.45$). The small circles represent the positions of K -band sources.

and SXDS1_60181) are ~ 1.3 – 1.6 , suggesting the presence of an overdense region by considering the uncertainty of photometric redshifts, although the apparent condensation of the galaxies may be chance coincidence. SXDS1_60394 with $z_{\text{phot}} = 2.37$ may be a background source. The expected number of K -band sources with $K_s \leq 23.55$ mag (the magnitude of the faintest source in this region) or with $K_s \leq 22.44$ mag (the magnitude of the faintest source excluding SXDS1_60394) which fall in an area with a radius of $5''$ is 0.7 and 0.3, respectively. In a similar way, the expected number of submm sources with $S_{1.3\text{mm}} \geq 0.2$ mJy is ~ 0.1 – 0.2 (based on the 1.3 mm number counts of Hatsukade et al. 2013). These suggest that this region has an excess of K -band sources and submm sources. AS5 appears to have a hint of tidal feature in the B -band image, suggesting an interaction. This region is also detected in *Spitzer* $24 \mu\text{m}$ and with *Herschel* (though as a single source due to its limited angular resolution), suggesting that the star-forming activity is increased. It is possible that these sources are a pre-merging system, and we may be witnessing the early phase of formation of a massive elliptical galaxy. Assuming that at least two sources including AS5 merge into a galaxy, the stellar mass would be 10^{11} – $10^{12} M_{\odot}$. It has been difficult to find such pre-merging systems in previous mm/submm observations due to the limited sensitivity and angular resolution before ALMA.

5. SUMMARY

We studied the optical–IR properties of 8 ALMA 1.3 mm faint sources detected in our deep observations in SXDS. We searched for K -band counterparts and found counterpart candidates for four ALMA sources within a radius of $0''.4$. The sum of probability of contamination by spurious sources for the 8 ALMA sources is ~ 1 , and it is likely that at least one of them is spurious. Possible reasons for no K -band counterparts are the ALMA detection is spurious, the optical/NIR color is bluer and faint in K_s , a larger offset between 1.3 mm emission and K_s -band emission, obscured by dust, and at higher redshift. While more than half of the ALMA-identified SMGs are above the main sequence, the ALMA serendipitous source is located in the main-sequence, suggesting that the ALMA-detected faint sources have properties similar to ‘normal’ star-forming galaxies. Comparison between K -band sources detected and undetected with ALMA within the field of views suggests that ALMA-detected sources tend to be brighter in K -band, more massive, and more actively star-forming galaxies.

We found a region where multiple ALMA sources and K -band sources reside within a radius of $5''$ and in a photometric redshift range of ~ 1.3 – 1.6 . This may be a pre-merging system and the early phase of formation of a massive elliptical galaxy.

We would like to acknowledge staffs at the ALMA Regional Center for their help in data reduction. BH is supported by JSPS KAKENHI Grant Number 15K17616. KO is supported by the Grant-in-Aid for Scientific Research (C)(24540230) from the Japan Society for the Promotion of Science. RM is supported by the Grant-in-Aid for JSPS Fellows. This paper makes use of the following ALMA data: ADS/JAO.ALMA#2011.0.00648.S. ALMA is a partnership of ESO (representing its member states), NSF (USA) and NINS (Japan), together with NRC (Canada), NSC and ASIAA (Taiwan), and KASI (Republic of Korea), in cooperation with the Republic of Chile. The Joint ALMA Observatory is operated by ESO, AUI/NRAO and NAOJ.

Facilities: ALMA.

REFERENCES

- Barger, A. J., Cowie, L. L., & Sanders, D. B. 1999, *ApJ*, 518, L5
 Blain, A. W., Smail, I., Ivison, R. J., Kneib, J.-P., & Frayer, D. T. 2002, *Phys. Rep.*, 369, 111
 Borys, C., Chapman, S., Halpern, M., & Scott, D. 2003, *MNRAS*, 344, 385
 Borys, C., Smail, I., Chapman, S. C., et al. 2005, *ApJ*, 635, 853
 Chen, C.-C., Cowie, L. L., Barger, A. J., Wang, W.-H., & Williams, J. P. 2014, *ApJ*, 789, 12
 Chen, C.-C., Smail, I., Swinbank, A. M., et al. 2015, *ApJ*, 799, 194
 Coppin, K., Chapin, E. L., Mortier, A. M. J., et al. 2006, *MNRAS*, 372, 1621
 da Cunha, E., Walter, F., Smail, I. R., et al. 2015, *ApJ*, 806, 110
 Daddi, E., Dickinson, M., Morrison, G., et al. 2007, *ApJ*, 670, 156
 De Breuck, C., Neri, R., Morganti, R., et al. 2003, *A&A*, 401, 911
 Dunne, L., Eales, S. A., & Edmunds, M. G. 2003, *MNRAS*, 341, 589
 Dye, S., Eales, S. A., Aretxaga, I., et al. 2008, *MNRAS*, 386, 1107
 Elbaz, D., Dickinson, M., Hwang, H. S., et al. 2011, *A&A*, 533, A119

- Fujimoto, S., Ouchi, M., Ono, Y., et al. 2015, arXiv:1505.03523
- Furusawa, H., Kosugi, G., Akiyama, M., et al. 2008, *ApJS*, 176, 1
- Greve, T. R., Ivison, R. J., Bertoldi, F., Stevens, J. A., Dunlop, J. S., Lutz, D., & Carilli, C. L. 2004, *MNRAS*, 354, 779
- Hainline, L. J., Blain, A. W., Smail, I., et al. 2011, *ApJ*, 740, 96
- Hatsukade, B., et al. 2011, *MNRAS*, 411, 102
- Hatsukade, B., Iono, D., Akiyama, T., et al. 2010, *ApJ*, 711, 974
- Hatsukade, B., Ohta, K., Seko, A., Yabe, K., & Akiyama, M. 2013, *ApJ*, 769, L27
- Hatsukade, B., Tamura, Y., Iono, D., et al. 2015, *PASJ*, in press (arXiv:1503.07997)
- Hildebrand, R. H. 1983, *QJRAS*, 24, 267
- Hodge, J. A., Karim, A., Smail, I., et al. 2013, *ApJ*, 768, 91
- Hodge, J. A., Riechers, D., Decarli, R., et al. 2015, *ApJ*, 798, LL18
- Hughes, D. H., Dunlop, J. S., & Rawlings, S. 1997, *MNRAS*, 289, 766
- Iono, D., Peck, A. B., Pope, A., et al. 2006, *ApJ*, 640, L1
- Ivison, R. J., Greve, T. R., Smail, I., et al. 2002, *MNRAS*, 337, 1
- Ivison, R. J., Smail, I., Dunlop, J. S., et al. 2005, *MNRAS*, 364, 1025
- Ivison, R. J., Greve, T. R., Dunlop, J. S., et al. 2007, *MNRAS*, 380, 199
- Ivison, R. J., Smail, I., Le Borgne, J.-F., et al. 1998, *MNRAS*, 298, 583
- Kennicutt, R. C., Jr. 1998, *ARA&A*, 36, 189
- Kimura, M., Maihara, T., Iwamuro, F., et al. 2010, *PASJ*, 62, 1135
- Lagache, G., Puget, J.-L., & Dole, H. 2005, *ARA&A*, 43, 727
- Lawrence, A., Warren, S. J., Almaini, O., et al. 2007, *MNRAS*, 379, 1599
- Lilly, S. J., Eales, S. A., Gear, W. K. P., et al. 1999, *ApJ*, 518, 641
- Le Floc'h, E., et al. 2005, *ApJ*, 632, 169
- McMullin, J. P., Waters, B., Schiebel, D., Young, W., & Golap, K. 2007, *Astronomical Data Analysis Software and Systems XVI*, 376, 127
- Michałowski, M., Hjorth, J., & Watson, D. 2010, *A&A*, 514, A67
- Noeske, K. G., Weiner, B. J., Faber, S. M., et al. 2007, *ApJ*, 660, L43
- Oke, J. B., & Gunn, J. E. 1983, *ApJ*, 266, 713
- Ono, Y., Ouchi, M., Kurono, Y., & Momose, R. 2014, *ApJ*, 795, 5
- Salpeter, E. E. 1955, *ApJ*, 121, 161
- Scott, K. S., Austermann, J. E., Perera, T. A., et al. 2008, *MNRAS*, 385, 2225
- Scott, K. S., et al. 2010, *MNRAS*, 405, 2260
- Simpson, J. M., Swinbank, A. M., Smail, I., et al. 2014, *ApJ*, 788, 125
- Smail, I., Chapman, S. C., Blain, A. W., & Ivison, R. J. 2004, *ApJ*, 616, 71
- Smail, I., Geach, J. E., Swinbank, A. M., et al. 2014, *ApJ*, 782, 19
- Symeonidis, M., Vaccari, M., Berta, S., et al. 2013, *MNRAS*, 431, 2317
- Takeuchi, T. T., Buat, V., & Burgarella, D. 2005, *A&A*, 440, L17
- Wang, W.-H., Cowie, L. L., van Saders, J., Barger, A. J., & Williams, J. P. 2007, *ApJ*, 670, L89
- Wiklund, T., Conzelice, C. J., Dahlen, T., et al. 2014, *ApJ*, 785, 111
- Yabe, K., Ohta, K., Iwamuro, F., et al. 2012, *PASJ*, 64, 60
- Yabe, K., Ohta, K., Iwamuro, F., et al. 2014, *MNRAS*, 437, 3647
- Younger, J. D., Dunlop, J. S., Peck, A. B., et al. 2008, *MNRAS*, 387, 707
- Younger, J. D., Fazio, G. G., Huang, J.-S., et al. 2007, *ApJ*, 671, 1531
- Younger, J. D., Fazio, G. G., Huang, J.-S., et al. 2009, *ApJ*, 704, 803

APPENDIX

TABLE 4
PHOTOMETRY OF ALMA-DETECTED SOURCES WITH *K*-BAND COUNTERPART CANDIDATES

Name	ID	<i>B</i>	<i>V</i>	<i>R</i>	<i>i</i>	<i>z</i>	<i>J</i>	<i>H</i>	<i>K_s</i>	3.6 μ m	4.5 μ m	5.8 μ m	8.0 μ m	24 μ m
ALMA_SXDS1_13015_1	AS1	24.63 \pm 0.02	24.28 \pm 0.02	23.75 \pm 0.03	23.16 \pm 0.01	22.41 \pm 0.01	21.17 \pm 0.01	20.52 \pm 0.01	20.00 \pm 0.00	19.32 \pm 0.00	19.19 \pm 0.00	19.36 \pm 0.03	19.40 \pm 0.03	194 \pm 6
ALMA_SXDS1_59863_1	AS4	25.19 \pm 0.04	24.68 \pm 0.03	24.60 \pm 0.06	24.08 \pm 0.02	23.62 \pm 0.03	22.39 \pm 0.03	21.89 \pm 0.04	21.28 \pm 0.02	20.45 \pm 0.01	20.19 \pm 0.01	20.01 \pm 0.05	20.52 \pm 0.09	-
ALMA_SXDS1_59863_2	AS5	24.12 \pm 0.01	23.89 \pm 0.02	23.33 \pm 0.02	22.84 \pm 0.01	22.23 \pm 0.01	21.15 \pm 0.01	20.57 \pm 0.01	20.19 \pm 0.01	19.62 \pm 0.01	19.49 \pm 0.01	19.74 \pm 0.04	19.73 \pm 0.04	-
ALMA_SXDS5_28019_1	AS8	24.30 \pm 0.01	24.08 \pm 0.02	23.57 \pm 0.02	23.28 \pm 0.01	22.67 \pm 0.01	22.00 \pm 0.02	21.53 \pm 0.02	21.16 \pm 0.01	20.65 \pm 0.01	20.61 \pm 0.01	21.19 \pm 0.13	21.55 \pm 0.19	41 \pm 4